Manuscript submitted to *Remote Sensing of Environment*

Assimilation of airborne gamma observations provides utility for snow estimation in forested environments

Eunsang Cho[1,2], Yonghwan Kwon[1,2*], Sujay V. Kumar[1], Carrie M. Vuyovich[1]

[1]Hydrological Sciences Laboratory, NASA Goddard Space Flight Center, Greenbelt, MD, USA
[2]Earth System Science Interdisciplinary Center, University of Maryland, College Park, MD, USA

[*]Corresponding author: Yonghwan Kwon (yonghwan.kwon@nasa.gov)

Submitted to *Remote Sensing of Environment*
Submission date: July 15, 2022

Abstract

An airborne gamma radiation technique provides a strong potential to estimate reliable snow water equivalent (SWE) in forested environments where remote sensing techniques typically have large uncertainties. This study explores the utility of assimilating the temporally (up to four measurements during a winter period) and spatially sparse airborne gamma SWE observations into a land surface model to improve SWE estimates in densely forested areas in the northeastern U.S. Here, we demonstrate that the airborne gamma SWE observations add value to the SWE estimates from the Noah land surface model with multiple parameterization options (Noah-MP) via assimilation despite the limited number of the measurements. Improvements are witnessed during the snow accumulation period while reduced skills are seen during the snow melting period. The efficacy of the gamma data is greater for areas with lower vegetation cover fraction and topographic heterogeneity ranges, and it is still effective in reducing the SWE estimation errors for areas with higher topographic heterogeneity. The gamma SWE data assimilation (DA) also shows a potential of extending the impact of flight line-based measurements to adjacent areas without observations by employing a localization approach. The localized DA reduces the modeled SWE estimation errors for adjacent grid cells up to 32-km distances from the flight lines. The enhanced performance of the gamma SWE DA is evident when the results are compared to those from assimilating the existing satellite-based SWE retrievals from the Advanced Microwave Scanning Radiometer 2 (AMSR2) for the same locations and time periods. Although there is still room for improvement, particularly for the melting period, this study shows that the gamma SWE DA is a promising method to improve the SWE estimates in forested areas.

Keywords

Snow water equivalent; Data assimilation; Airborne gamma radiation; Passive microwave; Land surface model

1 Introduction

Seasonal snowpack is an important freshwater resource in snow-dominated regions, and thus, accurate estimation of snow water equivalent (SWE), has been a pressing issue for managing water supply and forecasting snowmelt-driven flood events under the effects of climate change (Barnett et al., 2005; Sturm et al., 2017; Musselman et al., 2021). Due to its large variability, spatiotemporally continuous estimates of SWE cannot be generated by the existing in situ data network alone (e.g., Dozier, 2011). Large-scale distributions of SWE can be obtained from remote sensing data; however, these are subject to errors resulting from issues such as retrieval algorithm limitations and instrumental measurement noise. Land surface models (LSMs) provide spatially and temporally continuous estimates, but they suffer from large uncertainties associated with model physics, parameterizations, and meteorological boundary conditions. Given the limitations of each method, data assimilation (DA) has been considered as a promising alternative to improve the SWE estimation skill as it systematically merges remote sensing observations with LSM predictions.

Given the sensitivity to snow properties and long record of observations, passive microwave brightness temperature (T_B) observations have been used to retrieve SWE or snow depth (e.g., Change et al., 1990; Derksen et al., 2010; Foster et al., 2005; Kelly et al., 2003; Kelly, 2009), and used within data assimilation frameworks, for the assimilation of T_B (e.g., Durand and Margulis, 2006, 2007; Durand et al., 2009; Kwon et al., 2015, 2017; Larue et al., 2018a, 2018b; Xue et al., 2018) and assimilation of T_B-based retrievals of SWE or snow depth (e.g., Dong et al., 2007; Dziubanski and Franz, 2016; Kumar et al., 2014; Liu et al., 2013). However, in general, T_B-based approaches are considered suboptimal for the following surface conditions: (1) deep snow, (2) wet snow, and (3) dense forest. Many previous studies (e.g., Derksen et al., 2010; Kwon et al., 2019; Lemmetyinen et al., 2015) have reported that the T_B signal, especially at high frequency (e.g., 36.5 GHz), saturates in deep snowpacks (i.e., when SWE is greater than 100 to 200 mm), hampers microwave T_B-based SWE estimations. In the presence of wet snow, the T_B sensitivity to SWE decreases because liquid water dominates the T_B signal from the snowpack due to the high emissivity (approaches unity) of liquid water (Clifford, 2010; Walker and Goodison, 1993). Thus, the quality of the T_B-based SWE estimates is degraded under wet snow conditions (Kwon et al., 2019). The T_B sensitivity to SWE also diminishes in

densely forested areas (Roy et al., 2012) because the forest canopy blocks the microwave T_B emission from the snowpack and emits its own T_B signal (Foster et al., 1991), which adds considerable uncertainties in the T_B-based SWE estimates in dense forest (e.g., Kwon et al., 2016, Vuyovich et al. 2014). Vuyovich et al. (2014) showed specifically in the New England area that passive microwave retrievals underestimate SWE, though algorithms that account for forest fraction show improved performance. Although many enhancements have been proposed for the use of T_B observations in estimating SWE, there are still significant limitations to overcome.

Recently, airborne-based remote sensing approaches that have potential to overcome the existing challenges have been tested and used in assimilation schemes to improve snow depth or SWE (Light detection and ranging [lidar]; Hedrick et al., 2018; Smyth et al., 2019; 2020). Hedrick et al. (2018) focused on improvements to snow depth estimations over the Tuolumne River Basin in California by directly inserting the NASA Airborne Snow Observatory (ASO) airborne lidar data into the iSnobal model. They found that agreement between the lidar snow depth and updated modeled snow depth was greatly improved (r^2 = 0.90 and RMSE [root mean square error] = 12.5 cm) as compared to original modeled snow depth (r^2 = 0.16 and RMSE = 41.5 cm). Smyth et al. (2020) attempted to leverage snow depth observations with data assimilation (DA) to improve snow density and SWE estimations. They implemented a particle filter (PF) assimilation technique to assimilate the ASO lidar snow depth into the Flexible Snow Model. In this study, DA assimilation reduced snow density bias by over 40% and SWE bias by over 70% across eight climate zones in the western U.S. and in both wet and dry years. However, the impacts of known limitations such as forest cover and wet snow (in melting period) within a DA assimilation framework have not been widely examined. Smyth et al. (2020) also mentioned the impact of the limitations (e.g. cloud and forest cover) should be examined in future research. Furthermore, most studies have widely focused on the western U.S. environments (e.g. mountainous regions) with limited investigations in other regions such as temperate forest environments over northeastern U.S.

As a historically well-established remote sensing technique, the airborne gamma radiation technique provides a unique opportunity to estimate reliable SWE with minimal effects by wet snow and dense forest, because the gamma approach uses the attenuation of the terrestrial

gamma-ray emission by water in the snowpack (any phase) (Carroll, 2001; Carroll and Vose, 1984; Goodison et al., 1984). Since the early 1980s, airborne gamma radiation snow surveys operated by the National Oceanic and Atmospheric Administration's Office of Water Prediction (OWP; formerly by the National Operational Hydrologic Remote Sensing Center [NOHRSC]) have provided SWE observations to regional National Weather Service (NWS) River Forecast Centers (RFCs) and other federal agencies across the United States and southern Canada to help operational flood predictions and future water supply outlooks (Carroll, 2001; Peck et al., 1980). Recently, Cho et al. (2020b) found that the long-term gamma SWE record had remarkable agreement with ground-based gridded SWE products particularly in forested regions (R-value = 0.73 and 0.72 and Bias = 0.0 and -1.3 cm for mixed forest and deciduous forest, respectively), implying that the gamma radiation measurements have the potential to be used in a DA framework to improve estimation of SWE. Even though the airborne gamma radiation SWE products along with in-situ snow depth and SWE and satellite-based snow cover areas are currently assimilated into the National Weather Service (NWS) SNOw Data Assimilation System (SNODAS) to provide the near-real-time, high spatial resolution (1 km^2 gridded) SWE information (Barrett, 2003), how much the gamma radiation SWE retrievals help improve the modeled SWE estimates is not well quantified particularly in in a densely forested region.

The objective of this study is to evaluate the potential of the airborne gamma radiation SWE retrievals within a DA framework to enhance SWE estimates in a temperate forest environment in the northeastern U.S. We aim to answer three research questions: (1) How much is the modeled SWE improved by assimilating the airborne gamma SWE into the model? (2) Do land surface characteristics (e.g. forest density, slope, and elevation) affect the assimilation performance? (3) Can the spatial sparseness of the gamma SWE observations be overcome by employing the localized data assimilation approach? The Noah land surface model with multi-parameterization options (Noah-MP) is used to assimilate long-term airborne gamma radiation-based SWE observations with the ensemble Kalman filter scheme within the NASA Land Information System. This paper is organized as follows. Section 2 provides the study area with general land cover characteristics. Section 3 describes the datasets including the airborne gamma radiation survey, reference SWE data, tree cover fraction, and topographic feature variables. The description of the Noah-MP model with assimilation scheme is included in the section 4. Section 5 presents evaluation results of DA SWE performances with discussion about the similarities,

differences, and new findings in the results with respect to previous studies. Conclusion and future perspectives are drawn in section 6.

2 Study Area

The study area comprises parts of the northeastern United States, including New Hampshire and Maine with heavily forested regions which remain a challenging region in snow remote sensing and modeling communities. The dominant seasonal snow class in this region is montane forest (**Figure 1a**; Sturm & Liston, 2021). Land cover types are mainly deciduous broadleaf forest and mixed forest. Fractional tree cover (%) over the study area ranges from 70 to 100 % based on the vegetation continuous field (VCF) map from the NASA Making Earth System Data Records for Use in Research Environments (Hansen & Song, 2018; **Figure 1b**). The NOAA NOHRSC airborne gamma snow surveys occur almost every year over the designated flight lines (yellow lines). The airborne survey times range from 9 AM to 6 PM according to aircraft operation schedule and weather conditions (https://www.nohrsc.noaa.gov/snowsurvey/photos/).

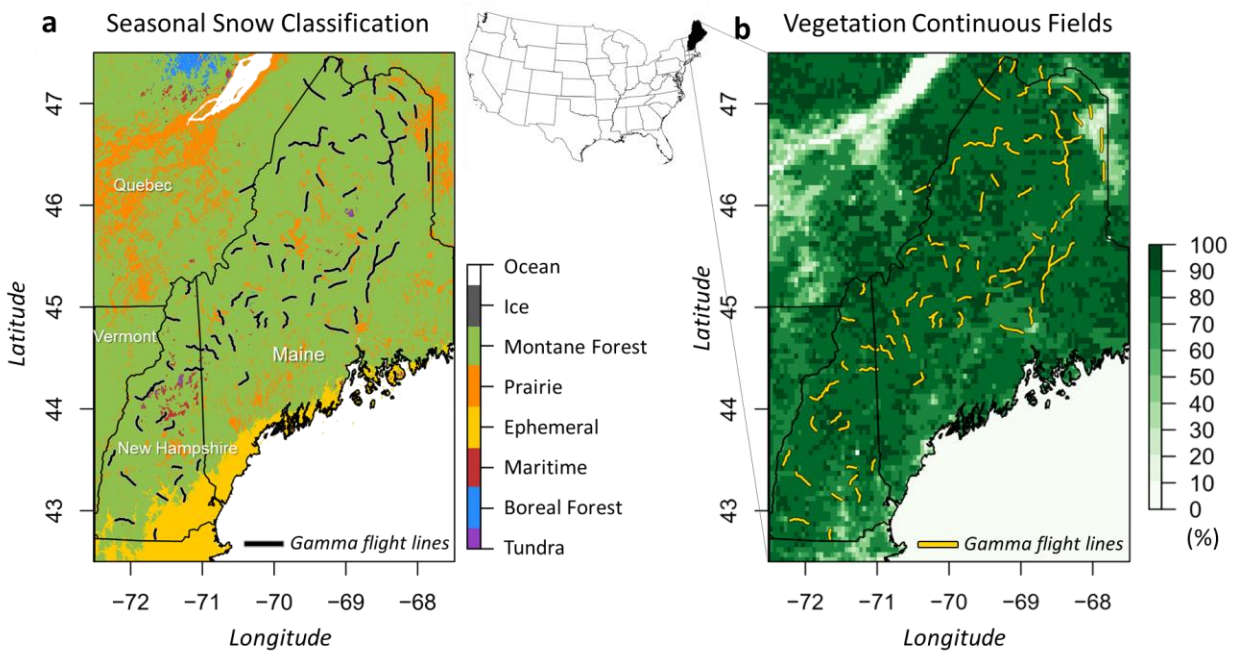

Figure 1. (a) Sturm and Liston's new seasonal snow classification (Sturm and Liston, 2021), and (b) Vegetation Continuous Field maps of the study area over the northeastern United States with the NOAA airborne gamma flight lines

3 **Data**

3.1 NOAA airborne gamma snow survey

The airborne gamma radiation snow and soil moisture survey operated by the NOAA's NOHRSC has been conducted throughout the United States and southern Canada to measure reliable SWE observations (Carroll, 2001). Since 1979, the operational gamma snow survey has provided over 27,000 gamma radiation SWE observations over the entire United States and southern Canadian provinces. The near real-time, airborne gamma SWE measurements have been successfully used by the National Weather Service (NWS) Hydrologic Services Program when issuing spring snowmelt flood outlooks, water supply outlooks, and river and flood forecasts. Also the airborne gamma SWE observations currently support the near-real-time, high spatial resolution (1 km^2 gridded) NOHRSC SNODAS (Barrett, 2003). The key principle of this technique is to use the attenuation of the gamma-ray signal by any phase of water in the snowpack (Carroll, 2001; Peck et al., 1980). The gamma radiation particles are observed using a gamma radiation detector onboard a low-flying aircraft at an altitude of 150 m. This detector measures terrestrial gamma radiation naturally emitted from trace elements of the three radioisotopes in the upper 20 cm of soil. The gamma SWE values are estimated using the difference between the rates of gamma radioisotopes ($^{40}K_0$, $^{208}Tl_0$, and gross count, GC_0) over bare ground and snow-covered ground (Cho et al., 2020a). The NOAA gamma flight lines are measured in the fall prior to freezing onset and then revisited in the winter to estimate SWE. The operational approach assumes the gamma rates over bare ground from the fall survey remain constant duringthe winter surveys. The airborne gamma SWE values are estimated using the following equations:

$$SWE(40K) = \frac{1}{A} \cdot \left[ln\left(\frac{40K_b}{40K_s}\right) - ln\left(\frac{100+1.11 \cdot SM(40K_s)}{100+1.11 \cdot SM(40K_b)}\right)\right] \quad (1)$$

$$SWE(208Tl) = \frac{1}{A} \cdot \left[ln\left(\frac{208Tl_b}{208Tl_s}\right) - ln\left(\frac{100+1.11 \cdot SM(208Tl_s)}{100+1.11 \cdot SM(208Tl_b)}\right)\right] \quad (2)$$

$$SWE(GC) = \frac{1}{A} \cdot \left[ln\left(\frac{GC_b}{GC_s}\right) - ln\left(\frac{100+1.11 \cdot SM(GC_s)}{100+1.11 \cdot SM(GC_b)}\right)\right] \quad (3)$$

where $^{40}K_b$, $^{208}Tl_b$, and GC_b and $^{40}K_s$, $^{208}Tl_s$, and GC_s are uncollided gamma count rates in the top 20 cm of soil over bare and snow-covered grounds, respectively. $SM(40K_b)$,

$SM(208Tl_b)$, and $SM(GC_b)$ and $SM(40K_s)$, $SM(208Tl_s)$, and $SM(GC_s)$ are the corresponding soil moisture values by weight (%). The operational airborne gamma radiation SWE (SWE_{gamma}; g/cm^2) is a weighted value by multiplying three independent SWE estimates by weighting coefficients, 0.346, 0.518, and 0.136, and summing the calculated values as below (Jones and Carroll, 1983; Carroll, 2001).

$$SWE_{gamma} = 0.346 \cdot SWE(40K) + 0.518 \cdot SWE(208Tl) + 0.136 \cdot SWE(GC) \quad (4)$$

The final SWE value is reported in the Standard Hydrometeorological Exchange Format (SHEF) product through the NOHRSC website (https://www.nohrsc.noaa.gov/snowsurvey/) (Carroll and Schaake Jr, 1983; Carroll, 2001). A typical flight path covers approximately 5 km^2 with a 300 m wide and 16 km long. The gamma SWE is an area-mean value for each flight path footprint. In this study for dense forest environments, 1,508 airborne gamma SWE observations covering 79 flight lines flown from January 1985 to May 2017 are used in the northeastern United States.

3.2 **UA SWE**

The UA SWE is used as reference data to evaluate and compare the open-loop and assimilation results from the Noah-MP simulations. The UA SWE is a ground observation-based 4-km gridded SWE product recently developed by consistently assimilating the snow telemetry (SNOTEL) SWE and NWS Cooperative Observer Program (COOP) snow depth measurements with the gridded PRISM precipitation and temperature data over the continental United States (Broxton et al., 2016a; Zeng et al., 2018). The accuracy and robustness of the UA SWE product as a reference continental snowpack data set have been proven by examinations including point-to- point and pixel- to- pixel interpolations (Broxton et al., 2016a, b), and evaluation against independent airborne snow observatory (ASO) lidar-based SWE and gamma radiation SWE measurements (Dawson et al., 2018; Cho et al., 2020b). Cho et al. (2020b) found that the UA SWE product strongly agreed with the 40-years airborne gamma SWE regardless of snow classification and land cover type over the continental U.S. This product has been used as a reference SWE for multiple purposes such as quantifying uncertainties in land surface modeled SWE (Kim et al., 2020; Zhang et al., 2022); characterizing extreme events (Welty and Zeng, 2021); developing “nature run” for observing system simulation experiments (Wrzesien et al.,

2021), and estimating extreme values for infrastructure design (Cho and Jacobs, 2020). In this study, the UA SWE product is used as reference data from October 1984 to December 2017. The product is freely available from the National Snow and Ice Data Center website (https://nsidc.org/data/nsidc-0719).

3.3 AMSR2 Passive Microwave SWE

For comparison purposes, the existing satellite-based SWE retrievals from the Advanced Microwave Scanning Radiometer 2 (AMSR2) are also assimilated in this study. AMSR2 is a passive microwave sensor that is the follow-on instrument to its predecessor, AMSR-E (Imaoka et al., 2010). As a part of the A-train constellation of the Earth observing satellites, AMSR2 has measured daily scans at 1:30 a.m./p.m. local time at 1–2 days revisit time since May 2012. The AMSR2 SWE product is generated based on the difference in brightness temperatures measured at 19.7 and 36.5 GHz along with higher and lower frequencies with snow density values for different snow classes based on the seasonal snow classification system. The SWE estimates are processed using the Kelly snow depth (SD) algorithm (Kelly, 2009). The Level 3 AMSR2 SWE products, expressed on the 10 km spatial grid, were acquired from the JAXA GCOM-W1 Data providing service (http://gcom-w1.jaxa.jp). To minimize the wet snow effects, this study used descending SWE data (01:30 a.m.) only.

3.4 **Tree cover fraction, and topographic features**

The NASA Making Earth System Data Records for Use in Research Environments (MEaSUREs) Vegetation Continuous Fields (VCF5KYR; Version 1) provides annual global fractional vegetation cover maps with three layers including percent tree cover, percent bare ground, and percent non-tree vegetation at 0.05 degree spatial resolution from 1982 to 2016 (Hansen and Song, 2018). In this study, the percent tree cover is used to evaluate the assimilation performance as a function of the tree cover fraction (TCF). To account for the interannual variations in the fractional tree cover, annual TCF values were obtained for each gamma SWE line. The elevation data (0.0083-degree spatial grid; approximately 1 x 1 km grid) used in this study were aggregated from the Shuttle Radar Topography Mission (SRTM) 90 m resolution elevation data (Farr et al., 2007). The slope and elevation range maps with the same spatial grid were obtained using the “terrain” function in the “raster” R-package (Wilson et al., 2007). The

elevation range (referred to as "topographic heterogeneity" in this paper) values were calculated as the difference between the aggregated minimum and maximum elevation value of a cell and its eight surrounding cells. The three topographic feature values were computed for each gamma flight footprint by a real-weighted average.

4 **Model and Methods**

4.1 Noah-MP

The Noah LSM with multi-parameterization options, version 3.6 (Noah-MP v3.6; Niu et al., 2011; Yang et al., 2011) was employed to simulate snow variables such as SWE and snow depth. Noah-MP was developed based on the original Noah LSM (Ek et al., 2003) with improved representations of biophysical and hydrological processes. A grid cell in Noah-MP consists of one vegetation canopy layer, up to three layers (depending on the total snow depth) of snowpack, four soil layers (with thicknesses of 0.1 m, 0.3 m, 0.6 m, and 1.0 m from top to bottom), and an unconfined aquifer layer. The model represents subgrid-scale land surface heterogeneity using a "semitile" scheme. In Noah-MP, a two-stream approximation (Dickinson, 1983; Sellers, 1985) is used to model incoming shortwave radiation by assuming that vegetation canopies are evenly distributed within a grid cell, whereas longwave radiation, latent heat flux, sensible heat flux, and ground heat flux are computed separately for vegetated and non-vegetated parts of a grid cell. Intercepted snow exists as solid and liquid phases on the vegetation canopy, and melting/refreezing of intercepted snow, dew/evaporation, and frost/sublimation on the vegetation canopy are explicitly modeled. Noah-MP simulates snow depth and SWE by considering snow layer compaction by the weight of the overlying snow layers, snow destructive and melt metamorphisms, and snowmelt-refreeze cycles. Snow layers are combined or subdivided based on prescribed layer thickness thresholds. Physical parameterization scheme options of Noah-MP v3.6 used in the current study are listed below: (1) dynamic vegetation for the vegetation option; (2) Noah-type soil moisture factor for stomatal resistance (Chen and Dudhia, 2001); (3) Ball-Berry canopy stomatal resistance scheme (Ball et al., 1987); (4) TOPMODEL- based runoff scheme; (5) simple groundwater scheme (SIMGM; Niu et al., 2007); (6) general Monin-Obukhov similarity theory (M-O; Brutsaert, 1982) for surface layer drag coefficient; (7) NY06 scheme (Niu and Yang, 2006) for supercooled liquid water (or ice fraction) in frozen soil; (8)

NY06 scheme (Niu and Yang, 2006) for frozen soil permeability; (9) modified two-stream radiation transfer scheme (Yang and Friedl, 2003, Niu and Yang, 2004); (10) Biosphere-Atmosphere Transfer Scheme (BATS) for ground surface albedo (Yang and Dickinson, 1996); (11) Jordan91 scheme (Jordan, 1991) for partitioning precipitation into rainfall and snowfall; (12) original Noah scheme for lower boundary condition of soil temperature; and (13) semi-implicit snow and soil temperature time scheme. An ensemble of model initial conditions was constructed through a two-step spin-up procedure. First, a single-member model simulation was run for 40 years, from 1 January 1980 to 1 January 2020, driven by the MERRA-2 (Modern-Era Retrospective analysis for Research and Applications, version 2; Bosilovich et al., 2015) forcing. Then, using a restart file generated in the first step, an additional 3-year spin-up, from 1 January 1981 to 1 March 1984, was conducted using 20 ensemble members. The open-loop (OL; without assimilation) and data assimilation (DA) experiments were run from 1 March 1984 to 1 October 2017 using the 20-member ensemble initial conditions. A model simulation time-step of 15 minutes was used, and daily mean outputs were evaluated.

4.2 Assimilation Scheme

Data assimilation experiments were conducted within the NASA Land Information System (LIS; Kumar et al., 2006; Peters-Lidard et al., 2007; Kumar et al., 2008). We applied the ensemble Kalman filter (EnKF) scheme (Reichle et al., 2002) to assimilate airborne gamma radiation-based SWE retrievals into Noah-MP. In the EnKF scheme, model uncertainty is implicitly represented by the ensemble spread (ensemble size of 20 was used in this study), which was generated by perturbing atmospheric forcing fields and model prognostic state variables (see **Table 1** for perturbation parameters) with the assumption of a Gaussian distribution. When observations (i.e., gamma SWE) are available, EnKF updates forecasted model state variables using the following equation:

$$M_i^{+} = M_i^{-} + K(Obs - HM_i^{-}) \quad (5)$$

where M_i^{+} is the updated (after assimilation) model states (i.e., SWE); M_i^{-} is the forecasted (before assimilation) model states (i.e., SWE); *Obs* is the gamma SWE retrievals; *H* is the observation operator (*H* = 1 in this study); *i* denotes the ensemble member; and *K* is the Kalman gain given by:

$$K = Cov(M_i^-, HM_i^-)\{Cov(HM_i^-, HM_i^-) + R\}^{-1} \quad (6)$$

where $Cov(M_i^-, HM_i^-) = Cov(HM_i^-, HM_i^-)$ is the covariance of the model forecasted SWE, and R is the covariance of the observation error. The gamma SWE retrieval error standard deviation of 23 mm was assumed based on Carroll and Vose (1984). Note that assimilation of gamma SWE updated only modeled SWE while snow ice and liquid water content, and snow depth were adjusted based on the SWE update by assuming that snow density does not change before and after the analysis update.

Table 1. Perturbation parameters applied to model prognostic state variables and atmospheric forcing fields during the OL and DA runs.

Variable	Perturbation Types	Std dev	AR(1)	Cross correlations		
Model prognostic state variables				*SWE*	*SD*	
SWE	M	0.01	3 hr	–	0.9	
Snow depth (*SD*)	M	0.02	3 hr	0.9	–	
Atmospheric forcing fields				*SW*	*LW*	*P*
Shortwave radiation (*SW*)	M	0.3	1 day	–	-0.5	-0.8
Longwave radiation (*LW*)	A	50 W m^{-2}	1 day	-0.5	–	0.5
Precipitation (*P*)	M	0.5	1 day	-0.8	0.5	–

M: multiplicative; A: additive; AR(1): first-order autoregressive temporal correlation.

4.3 DA localization

A limitation of using the airborne gamma radiation-based SWE observations within the DA system is its sparsity in space and time. Assimilating the temporally sparse gamma SWE observations can still improve the modeled SWE for flight lines as presented in section 5. Here we also address the feasibility of extending the impact of flight line-based gamma SWE observations to adjacent grid cells, where the observations are not available, through a simple approach. That is, the amount of the analysis updates of the SWE estimates calculated during the assimilation procedure for the flight lines are added to other grid cells within a specified distance from the flight lines by applying a localization weight (W), which is calculated using a distance-based localization method using the Gaussian decay:

$$W = exp\left\{\frac{-d^2}{2\cdot\left(\frac{r}{2}\right)^2}\right\} \quad (7)$$

where d is the physical distance between the updated grid cells (i.e., flight lines) and grid cells without observations within a specified localization radius r. If a grid cell is affected by multiple flight lines, the averaged amount of the updates is added to the prior SWE estimates of the grid cell. In this study, we apply a localization function with six different distances (e.g., 4, 8, 16, 24, 32, and 48 km from the lines). For an evaluation of the DA SWE with the localization weight, the areal mean DA SWE time series are obtained for an effective area buffered by a specified distance around the gamma flight line. To compare this with the corresponding OL and UA SWE values, the areal mean OL and UA SWE time series are obtained in the same way.

5 **Results and discussion**

5.1 Comparison between DA and OL SWE with airborne gamma SWE

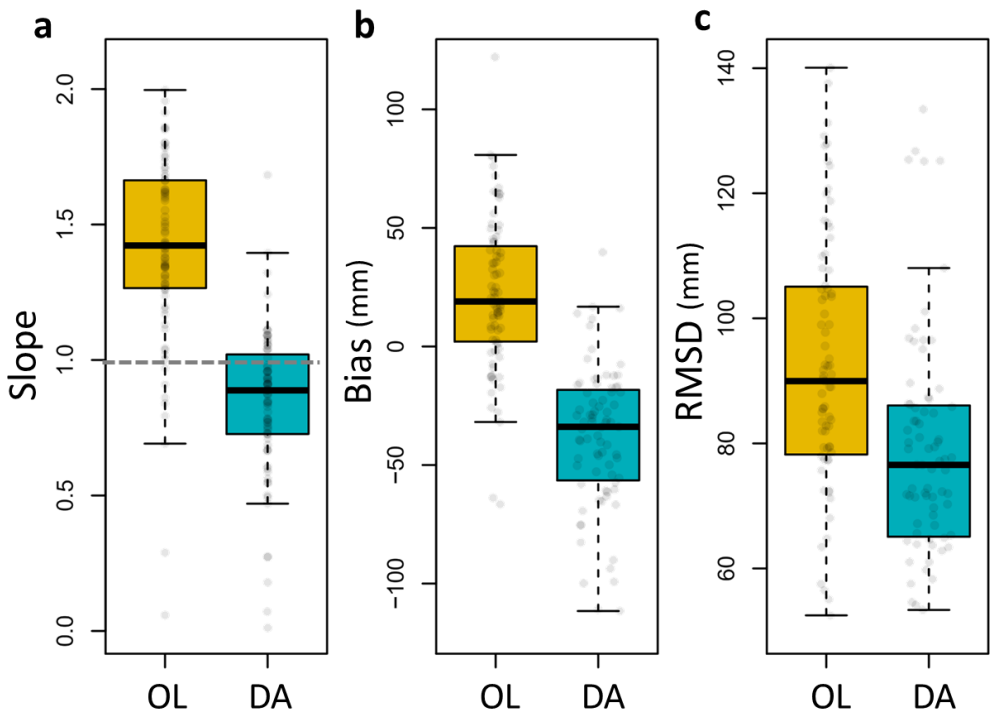

Figure 2. Comparison of statistics between open-loop (OL) SWE and data assimilated (DA) Noah-MP SWE estimates by using airborne gamma radiation SWE observations with the

University of Arizona SWE from 1985 to 2017: (a) slope from 1:1 plot, (b) Bias, and (c) RMSE from a linear relationship between the estimated SWE and UA SWE.

To examine the updated SWE performance over the gamma lines by assimilating airborne gamma observations into Noah-MP, statistical metrics were compared between OL and DA SWE using UA SWE (**Figure 2**). The values of 1:1 slope were closed to 1 (A median slope of OL was 1.45) and RMSD values decreased, even though negative biases were found. The lower bias of the SWE estimates from the OL as compared to the DA in **Figure 2** was a

consequence of the fact that the overestimated SWE during the accumulation season and early in the melt season was offset by the underestimated SWE during the snowmelt season (i.e., April and May). When the gamma SWE observations exist during the accumulation period (which is a typical case), DA corrected the overestimated SWE, whereas it further underestimated SWE in the snowmelt season (**Figures 3** and **4**), resulting in the increased (negative) bias, as presented in **Figure 2**. The OL SWE was largely deviated from the 1:1 linear relationship during the snow accumulation season (i.e., January, February, and March) and early in the snowmelt season (i.e., April). **Figure 3** shows that the deviation was significantly reduced through the assimilation of the gamma SWE retrievals even though a reduced R-value was obtained.

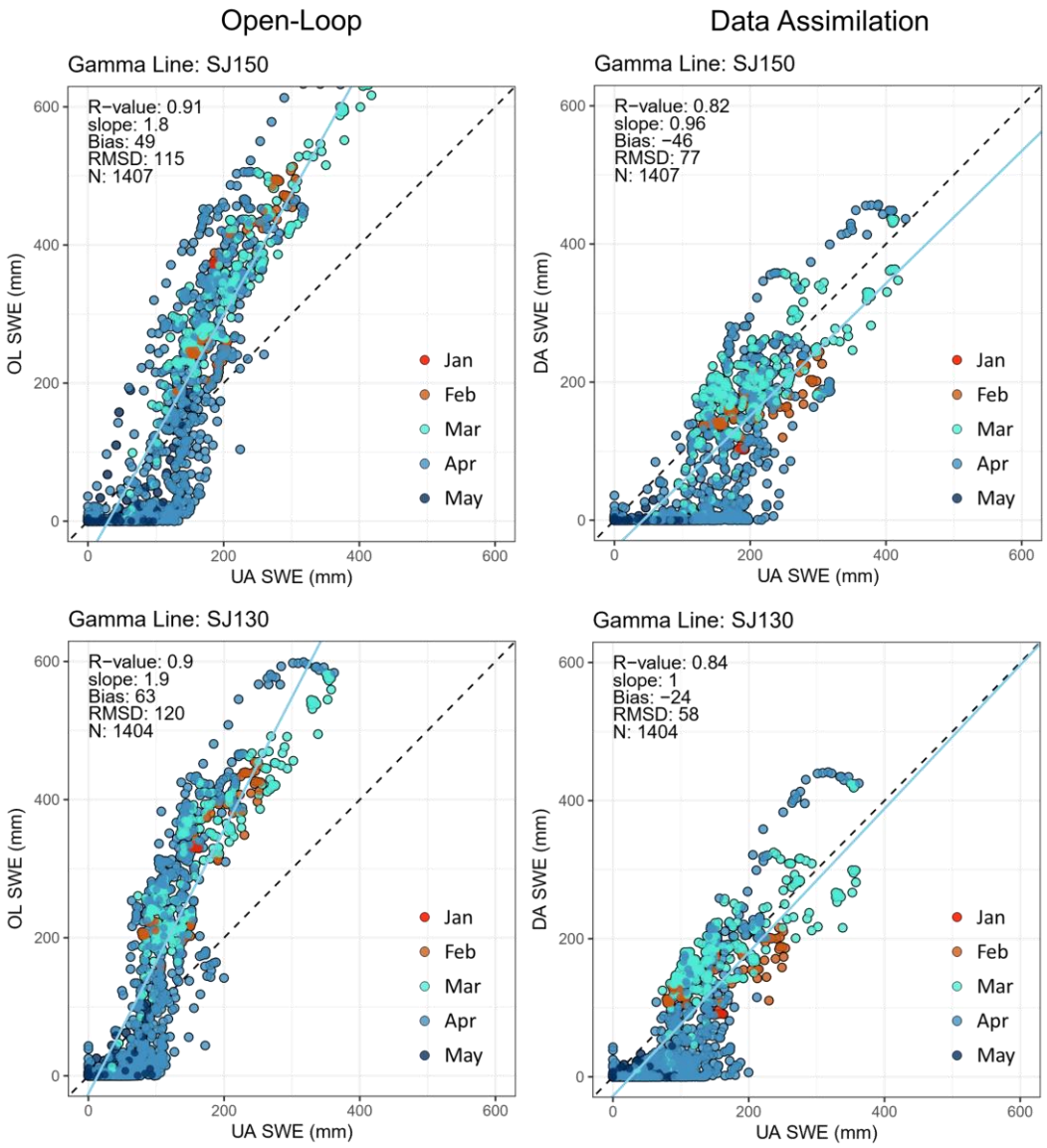

Figure 3. Examples of scatterplots of two gamma flight lines (SJ150 and SJ203) between the Noah-MP SWE estimates (from the open-loop (OL) and data assimilation (DA) experiments; y-axis) and daily University of Arizona SWE (x-axis) from October 1985 to May 2017 (total 33 water years). R-value, slope, Bias, RMSD, and number of data points (N) in the linear relationship are presented in the figures.

A promising aspect is that the assimilation of the temporally sparse (i.e., only one or two data points at the end of the snow accumulation period and/or early in the snowmelt period) airborne gamma SWE retrievals enhanced the model estimates of SWE, which was particularly noticeable in some lines and years, such as the gamma line SJ150 in WY1991 (**Figure 4**). For comparison purposes, results of assimilating the AMSR2 SWE retrievals were also plotted (green solid line in **Figure 4**). As shown in the figure, the AMSR2 SWE was largely deviated

(underestimated) from the UA SWE in densely forested areas, and assimilating the AMSR2 SWE data led to degradation of the SWE estimates. This further emphasizes the effectiveness of the gamma SWE data in improving the model estimates of SWE via assimilation in forested areas even with fewer available data compared to the AMSR2 SWE. However, the assimilation of the airborne gamma SWE measurements was not able to improve the snow ablation timing probably due to temporally sparse gamma data as well as limited model physics. As shown in **Figure 4**, compared to the UA SWE, Noah-MP simulated earlier snow melt-out despite the overestimated snow accumulation, which may be attributed to the Noah-MP model structure and physics (e.g., simplified representations of snow layers). The availability of more frequent gamma observations during the snowmelt season could lead to further improvements in estimating SWE in the ablation period while the Noah-MP snow layer representation needs to be enhanced.

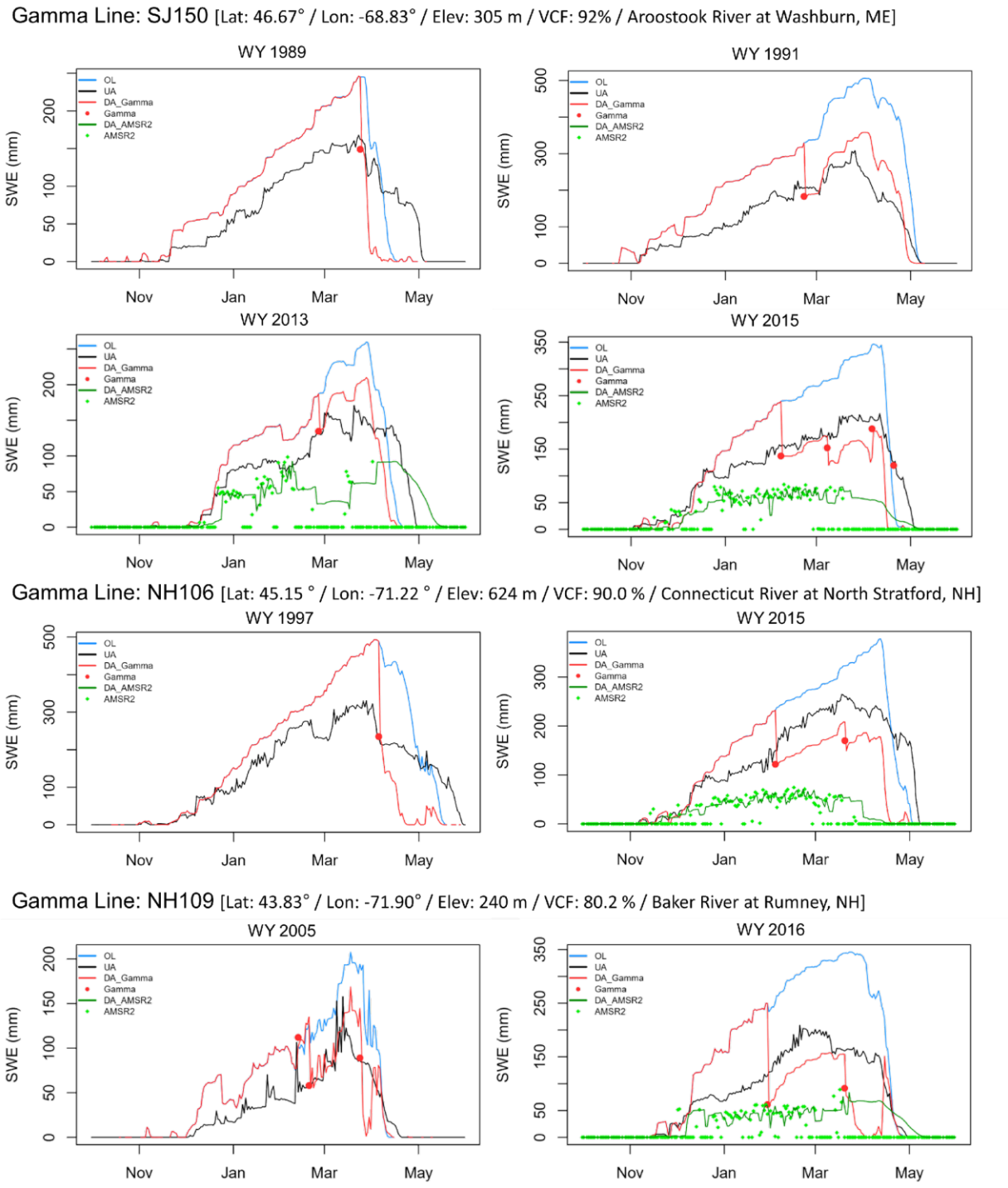

Figure 4. Examples of daily SWE time series of three gamma lines (SJ150, NH106, and NH109) with latitude (Lat), longitude (Lon), elevation (Elev), and vegetation cover fraction (VCF) for individual years including the open-loop (OL) and gamma data assimilated (DA_Gamma) Noah-MP SWE estimates along with the passive microwave SWE data from the Advanced Microwave Scanning Radiometer 2 (AMSR2) and AMSR2 data assimilated SWE (DA AMSR2).

5.2 Effect of land surface characteristics on assimilation performance

To examine effects of land surface characteristics on the DA performances as compared to the OL, the performance of the gamma SWE DA, presented as differences (i.e., DA minus OL) in the 1:1 slope, bias, and RMSD, with the UA SWE were compared by four physical features, TCF, slope, elevation range (i.e., topographic heterogeneity), and elevation (**Figure 5**). In the figure, two groups of each land surface characteristics were determined by dividing the gamma flight lines into two (i.e., low and high) groups of equal numbers of the flight lines. For TCF, DA SWE in a group with low TCF (less than 85%) has lower bias and RMSD than OL SWE, while the DA performances show relatively marginal improvement in the high TCF. Considering that the TCF values in the low group ranges from 31% to 84% (mean: 62 %), DA using airborne gamma SWE improved SWE over densely forested regions.

Differences in the DA performance between the low and high groups were observed for all surface characteristics. The 1:1 slope was updated by DA for both the lower and higher ranges of all surface characteristics. DA led to larger improvements in the 1:1 slope and RMSD for lower VCF, slope, elevation range, and elevation. With respect to the bias, assimilation of the gamma SWE retrievals improved the group-averaged performance for both the lower and higher groups of the surface characteristics with larger improvement in lower VCF and higher slope, elevation range, and elevation. For individual physical characteristics, the added value of the gamma SWE data on the model SWE estimates via assimilation was greater for the lower VCF range based on both bias and RMSD. It is worth noting that the lower VCF ranges from 31% to 84%, and DA significantly improved the SWE, even for the higher VCF (i.e., greater than 85%). This implies that the gamma-based SWE estimates within DA frameworks can be a promising alternative to traditional T_B-based approaches in forested areas. Comparable DA performance patterns were also obtained for other land surface characteristics. Although the gamma SWE DA exhibited smaller RMSD improvements in areas with higher topographic heterogeneity, than those with lower ranges, it was still effective in reducing error statistics.

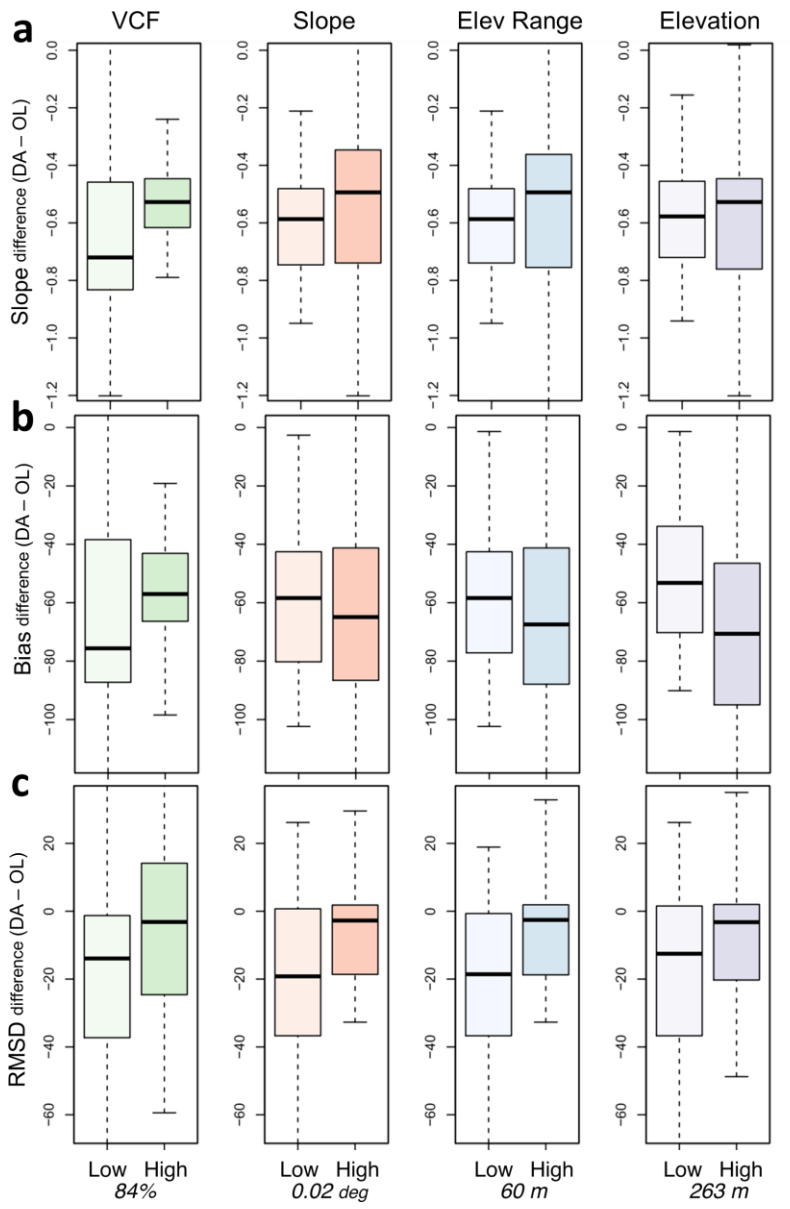

Figure 5. Boxplots of differences in (a) Slope from 1:1 plot, (b) Bias, and (c) RMSD between the DA and OL cases (computed as DA – OL) with respect to vegetation cover fraction (VCF), slope (degree), elevation range (m), and elevation (m). The two groups (low/high) were divided into equal numbers of values. The bottom values are 50% quantile values for each characteristic.

5.3 Localized data assimilation (DA) performance

One of the limitations of the airborne gamma SWE observations is a limited spatial coverage, which is typically 5-7 km^2 with a swath 300 m wide and 15-30 km long. It is necessary to assess if the spatially sparse airborne gamma SWE observations can also improve the SWE estimates in the surrounding areas, where gamma flights do not exist, via assimilation. Here, the

DA experimental cases that employ a localization function with different distances (e.g., 4, 8, 16, 24, 32, and 48 km from the flight lines) are evaluated (**Figure 6**). The OL/DA statistics in the figure are calculated using domain-averaged time series of OL/DA SWE over the effective surrounding areas by localization distances with the corresponding UA SWE. For the whole snow season that includes both accumulation and melting periods, the boxplot of the 1:1 slope shows that the localized DA SWE were remarkably improved as compared to OL. The slope of the DA SWE is closed to 1 by up to 32 km distance while the OL's slope continually increased by up to 1.4, indicating an overestimation of 40%. The RMSD boxplot also shows that the DA SWE has lower errors than the OL SWE for all localization distances, except 4 km. The OL's RMSD increased with increasing the distances up to 16 km (median: 66 mm) and above that, the differences remain approximately constant, while the DA's RMSD values slightly decreased with increasing the distances up to 32 km (median: 53 mm). When the statistics were calculated for the accumulation and melting periods separately, the lower RMSDs and slopes closer to 1 of the localized DA SWE were found consistently. As previously discussed, the efficacy of assimilating the airborne gamma SWE is greater during the accumulation period, especially for bias and RMSD, than during the melting period. Even in the melting period, some improvements in the RMSD and 1:1 slope with longer distances are achieved.

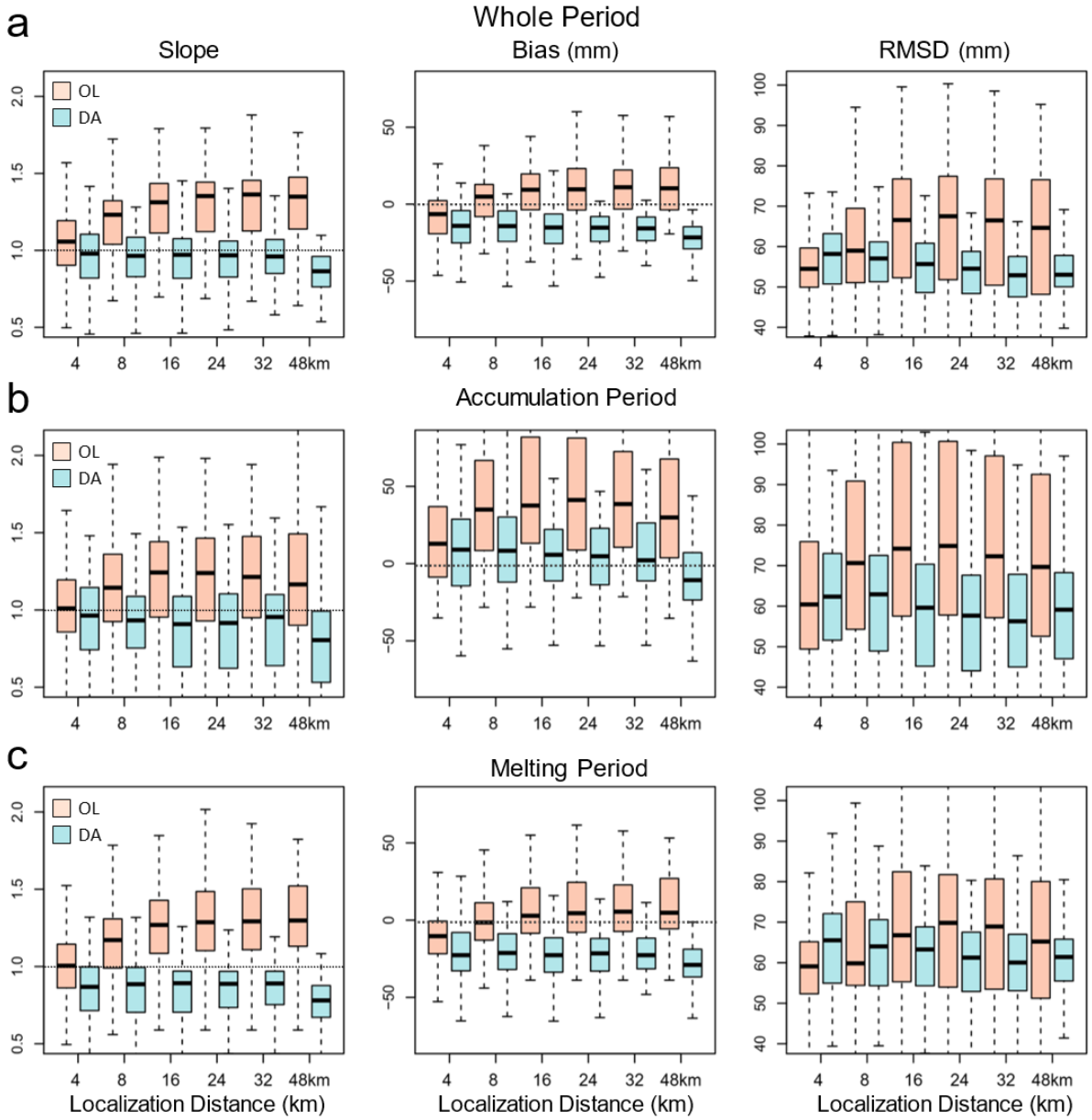

Figure 6. Localized data assimilation (DA) and open-loop (OL) Noah-MP SWE performances as compared to the UA SWE with different localization distances (e.g., 4, 8, 16, 24, 32, and 48 km) for the whole (accumulation and melting periods), accumulation, and melting periods, respectively.

The localized gamma DA outputs using the 32-km localization distance are compared with the AMSR2 DA outputs (**Figure 7)**. Because the AMSR2 SWE was largely underestimated in the study domain (see **Figure 4**), assimilating the AMSR2 SWE measurements did not improve the modeled SWE estimates. All error metrics of the AMSR2 DA SWE were degraded (e.g. median bias: 160 mm and RMSD: 175 mm) as compared to the OL (bias: 49 mm and

RMSD: 76 mm). The localized gamma DA SWE performance is clearly improved based on the error metrics. The positive biases (median: 50 mm) and high slopes of the OL SWE were improved, and the RMSD also decreased approximately by 25 mm.

Overall, we found that the localized DA using the airborne gamma SWE observations reduced the model SWE's errors up to 32 km distances, which is supported by the recent study that a single gamma SWE observation spatially represents up to 50 km even in dense temperature forest environments (Cho et al., 2022). The study found that there was strong agreement between the gamma SWE observations and in-situ snow course transects (R-value: 0.78; RMSD: 53 mm) at distances up to 50 km in the northeastern U.S. The results in this study indicate that, even though the airborne gamma SWE measurements exist with limited spatial coverages, the combined use of the physical model and DA with the gamma SWE has a potential to improve regional estimations of the SWE.

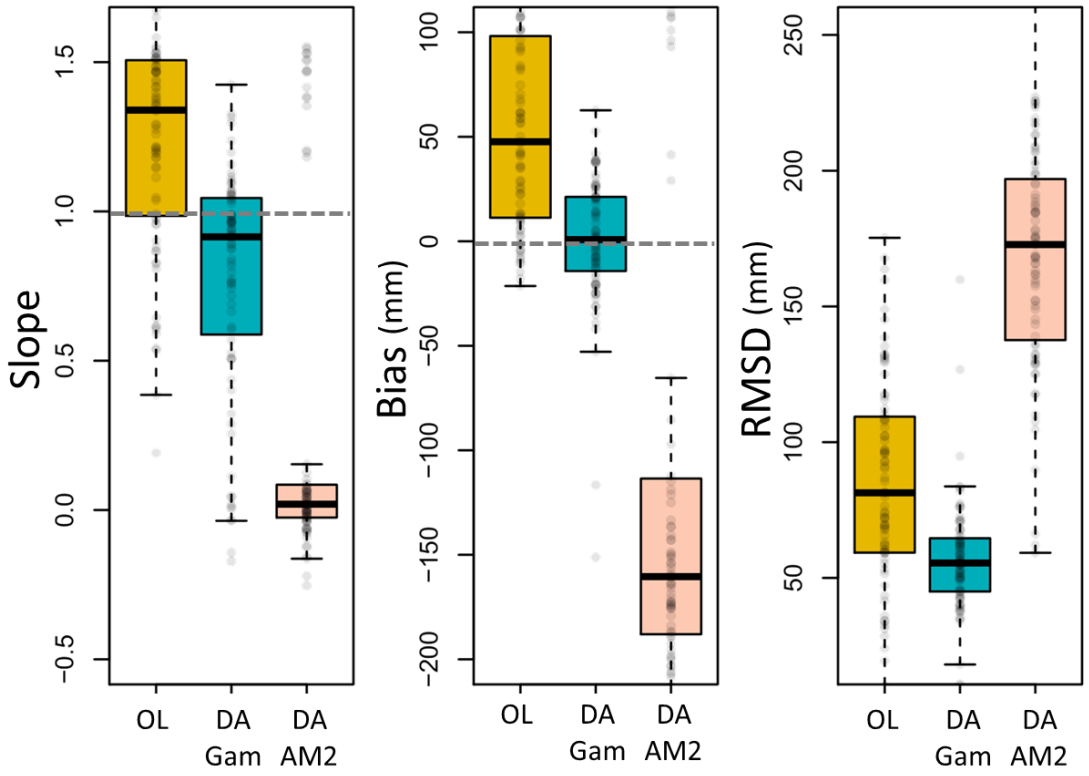

Figure 7. Comparison of the SWE estimation performance between the open-loop (OL), gamma DA, and AMSR2 DA as compared to the UA SWE at the 32km localization distance for the mutual DA effective accumulation periods.

6. Limitations

We observed two issues associated with the Noah-MP SWE estimates in the study domain: 1) Noah-MP considerably overestimated SWE during the snow accumulation period; while 2) it underestimated SWE (i.e., early snowmelt) during the snow ablation period (see **Figure 4**). The former issue was mitigated through the assimilation of the gamma SWE retrievals, whereas the latter issue was not. The overestimated SWE during the snow accumulation period was likely attributed to a precipitation phase partitioning method employed in Noah-MP. Given the same amount of total precipitation, different phase partitioning methods lead to substantial differences in the amount of snowfall (Xia et al., 2017; Jennings et al., 2018; Suzuki and Zupanski, 2018; Letcher et al., 2021). Noah-MP uses the scheme of Jordan (1991), in which total precipitation is fractionally divided into rainfall and snowfall using two thresholds of air temperature (i.e., no snowfall when Tair > 2.5℃; all precipitation is snow when Tair ≤ 0℃; and fractional snowfall when 0℃ < Tair ≤ 2.5℃). However, Noah-MP uses a spatially uniform threshold of T_{air}. Jennings et al. (2018) found that rain-snow T_{air} thresholds exhibited significant spatial variability across the Northern Hemisphere with the warmest thresholds in continental and mountain areas while with the coolest thresholds in maritime areas and lowlands. This implies that the high T_{air} threshold (i.e., 2.5℃) used in Noah-MP may lead to the overestimated snowfall, and subsequently the overestimated snow depth and SWE as the study area is characterized by maritime. Letcher et al. (2021) demonstrated that the use of cooler T_{air} thresholds in Noah-MP can significantly improve the estimates of peak SWE in the northeastern United States. The SWE estimates of Noah-MP with the assimilation of the gamma SWE retrievals can be further improved by using more refined precipitation phase partitioning methods that consider both air temperature and humidity as suggested in Jennings et al. (2018).

Simplified snow layering schemes (i.e., single snow layer) with the assumption of the same snow density for the entire snow column cause rapid snowmelt (e.g., Kwon et al., 2014; Suzuki and Zupanski, 2018). Although the snowpack in Noah-MP can have up to three snow layers, it may not be enough to accurately reproduce the energy budget within the snowpack in the study area. Further improvement in the modeled SWE during the melting season can be achieved by employing a more sophisticated snow model. Meanwhile, the current DA framework does not perform assimilation if one or more of the prior model ensemble members

do not have snow. Thus, the gamma SWE retrievals could not add value to the SWE estimates during the snow melting period. To address this issue, a rule-based approach (e.g., Kwon et al., 2019), that adds a thin snow layer when the model simulates snow-free conditions, but observations have snow, can be explored in a future study.

While the airborne gamma radiation SWE was used to enhance SWE estimations by assimilating into Noah-MP land surface models, it is possible that the inherent uncertainties in the gamma radiation method limit the potential improvements through DA. The potential sources of error in the gamma SWE retrievals have been explored in previous findings (Carroll & Carroll, 1989a, 1989b; Glynn et al., 1988; Offenbacher & Colbeck, 1991). An impact of forest biomass on the accuracy of airborne gamma SWE measurements has been examined over forested watersheds (Carroll & Vose, 1984; Vogel et al., 1985). Carroll and Vose (1984) presented that there was 23 mm of RMSE between airborne gamma SWE and in-situ SWE for the moderate snowpack (20 to 470 mm of in-situ SWE) in Lake Superior and Saint John basins, New Brunswick, Canada. Spatial variability in elevations over the gamma flight footprint can cause larger errors in SWE (Cho et al., 2020b; Carroll & Carroll, 1989b; Cork & Loijens, 1980). Cho et al. (2020b) found that heterogeneous characteristics (e.g. elevation range and slope) within a flight line cause underestimates of gamma SWE as compared to UA SWE. Cork & Loijens (1980) discussed that the measurements of the attenuation of the gamma count rate over the snowpack with its large spatial variability were systematically underestimated leading to the SWE underestimation. Because the results use the NOAA standard gamma radiation SWE retrievals without manual corrections, the DA results would be improved with the updated gamma SWE products in regions by correcting the existing potential errors. Lastly, the spatiotemporal sparseness of the airborne gamma SWE observations due to the operational costs is an inherent issue that may limit the widespread use of gamma SWE observations for DA work. However, as proven in our findings, effective uses of the gamma SWE (e.g. localization function) will maximize the utility of the gamma SWE into the DA framework.

7 Conclusion and Future Perspectives

In the snow hydrology community, DA has been used as a promising alternative to improve SWE estimation at a large spatial scale by merging remote sensing observations with

LSM predictions. In densely forested regions, however, most remote sensing techniques have limited performance of SWE due to attenuating or/and scattering radiation signals by canopy (e.g. passive microwave T_B and Lidar), resulting in large uncertainty in DA outputs. The historically well-established, airborne gamma radiation technique has provided a strong potential in wet snow and dense forest conditions, because the gamma approach uses an attenuation difference in the terrestrial gamma-ray emission by water in the snowpack (any phase) between snow-off and snow-on conditions. In this study, the airborne gamma SWE observations are assimilated with the Noah-MP model's SWE in densely forested regions in the northeastern U.S. We found that the assimilation of the airborne gamma SWE observations enhanced the model SWE estimates despite the limited number of the measurements (up to four SWE values during a winter period). The added value of the gamma data on the model SWE estimates was greater for the relatively lower VCF range. For areas with higher topographic heterogeneity, the gamma-based DA SWE was still effective in reducing the errors. We also found that the localized DA with the gamma SWE observations with distances up to 32 km reduced the model SWE's errors, indicating the gamma SWE has a potential to improve regional estimations of the SWE and subsequently snowmelt runoff. Despite the accuracy of the gamma data on the DA framework, the improvements were limited by the spatial and temporal sparseness of the gamma measurements and the uncertainties in the Noah-MP physics (i.e. precipitation partitioning and simplified snow layers). With the enhanced physics in LSMs and optimal uses of the gamma data using enhanced DA/interpolation methods, future studies may achieve a further improvement of the modeled SWE for larger areas where gamma flights do not exist.

Acknowledgments

The authors gratefully acknowledge support from NASA Terrestrial NASA Hydrology (THP) Program (NNH16ZDA001N). We are grateful to the NOAA NWS NOHRSC colleagues (Tom Carroll, Don Cline, and Carrie Olheiser) for the dedication and steady efforts to operate the airborne gamma snow survey. The airborne gamma radiation SWE data are freely available from the NOAA NWS NOHRSC website (http://www.nohrsc.noaa.gov/snowsurvey/). The UA daily 4-km SWE data (Version 1) and JAXA AMSR2 L3 Global Daily 10 km SWE data (Version 1) are available from the website (https://nsidc.org/data/nsidc-0719 and https://gportal.jaxa.jp/gpr/information/download, respectively).

References

Ball, J. T., Woodrow, I. E., & Berry, J. A. (1987). A model predicting stomatal conductance and its contribution to the control of photosynthesis under different environmental conditions. In *Progress in Photosynthesis Research*; Biggins, J., Ed.; Martinus Nijhoff: Dordrecht, Netherlands, pp. 221–234. https://doi.org/10.1007/978- 94- 017- 0519- 6_48

Barnett, T. P., Adam, J. C., & Lettenmaier, D. P. (2005). Potential impacts of a warming climate on water availability in snow-dominated regions. *Nature*, 438(7066), 303-309.

Barrett, A. P. (2003). National Operational Hydrologic Remote Sensing Center Snow Data Assimilation System (SNODAS) products at NSIDC (p. 19). Boulder, CO: National Snow and Ice Data Center, Cooperative Institute for Research in Environmental Sciences

Beck, H. E., Zimmermann, N. E., McVicar, T. R., Vergopolan, N., Berg, A., & Wood, E. F. (2018). Present and future Köppen-Geiger climate classification maps at 1-km resolution. *Scientific data*, 5, 180214.

Bosilovich, M. G., Lucchesi, R., & Suarez, M. (2015). MERRA-2: File specification. *NASA GMAO Office Note* 2015, 9, 73 pp. [Available online at http://gmao.gsfc. nasa.gov/pubs/docs/Bosiloich785.pdf].

Broxton, P., Dawson, N., & Zeng, X. (2016a). Linking snowfall and snow accumulation to generate spatial maps of SWE and snow depth. *Earth and Space Science*, 3, 246–256. https://doi.org/10.1002/2016EA000174

Broxton, P., Zeng, X., & Dawson, N. (2016b). Why do global reanalyses and land data assimilation products underestimate snow water equivalent? *Journal of Hydrometeorology*, 17(11), 2743–2761. https://doi.org/10.1175/JHM-D-16-0056.1

Brutsaert, W.A. (1982). Evaporation into the Atmosphere; D. Reidel: Dordrecht, The Netherlands.

Carroll, T. R. (1981). Airborne soil moisture measurement using natural terrestrial gamma radiation. *Soil Science*, 132(5), 358-366.

Carroll, T. R. (2001). Airborne Gamma Radiation Snow Survey Program: A User's Guide, Version 5.0. National Operational Hydrologic Remote Sensing Center (NOHRSC), Chanhassen, 14

Carroll S. S. & Carroll T. R. (1989a), Effect of forest biomass on airborne snow water equivalent estimates obtained by measuring terrestrial gamma radiation. *Remote Sensing of Environment*, 27(3), 313–319.

Carroll S. S., & Carroll T. R. (1989b), Effect of uneven snow cover on airborne snow water equivalent estimates obtained by measuring terrestrial gamma radiation. *Water Resources Research*, 25 (7):1505–1510.

Carroll, T. R. & Schaake Jr, J. C. (1983). Airborne snow water equivalent and soil moisture measurement using natural terrestrial gamma radiation. *In Optical Engineering for Cold Environments* (Vol. 414, pp. 208-214). International Society for Optics and Photonics.

Carroll, T. R. & Vose, G. D. (1984). Airborne snow water equivalent measurements over a forested environment using terrestrial gamma radiation. *In Proceedings of the Eastern Snow Conference*, 29, 101-115.

Chang, A., Foster, J., & Hall, D. (1990). Satellite sensor estimates of northern hemisphere snow volume. *International Journal of Remote Sensing*, 11(1), 167−171. https://doi.org/10.1080/01431169008955009

Chen, F., & Dudhia, J. (2001). Coupling an advanced land surface- hydrology model with the Penn state- NCAR MM5 modeling system. Part I: Model implementation and sensitivity.

Monthly Weather Review, 129(4), 569–585. https://doi.org/10.1175/1520-0493(2001)129<0569:CAALSH>2.0.CO;2

Cho, E., & Jacobs, J. M. (2020). Extreme Value Snow Water Equivalent and Snowmelt for Infrastructure Design over the Contiguous United States. *Water Resources Research*, 56(10), e2020WR028126.

Cho, E., Jacobs, J. M., Tuttle, S. E., Schroeder, R., & Olheiser, C. (2020a). Improvement of Airborne Gamma Radiation Snow Water Equivalent Measurements Using SMAP Soil Moisture, *Remote Sensing of Environment*, 240, https://doi.org/10.1016/j.rse.2020.111668

Cho, E., Jacobs, J. M., & Vuyovich, C. (2020b). The value of long- term (40 years) airborne gamma radiation SWE record for evaluating three observation- based gridded SWE datasets by seasonal snow and land cover classifications. *Water Resources Research*, 56(1), e2019WR025813. https://doi.org/10.1029/2019WR025813

Cho, E., Mortimer, C., Mudryk, L., Derksen, C., Vuyovich, C., Brady, M. (2022). Quantifying Spatial Representativeness of Airborne Gamma Radiation SWE using Snow Courses and Gridded Reanalysis data, *AMS Annual Meeting 2022*.

Clifford, D. (2010). Global estimates of snow water equivalent from passive microwave instruments: History, challenges and future developments. *International Journal of Remote Sensing*, 31(14), 3707–3726. https://doi.org/10.1080/01431161.2010.483482

Cork, H. F., & Loijens, H. S. (1980). The effect of snow drifting on gamma snow survey results. *Journal of Hydrology*, 48(1-2), 41-51.

Daly, C., Halbleib, M., Smith, J. I., Gibson, W. P., Doggett, M. K., Taylor, G. H., et al. (2008). Physiographically sensitive mapping of climatological temperature and precipitation across the conterminous United States. *International Journal of Climatology: a Journal of the Royal Meteorological Society*, 28(15), 2031-2064.

Dawson, N., Broxton, P., & Zeng, X. (2017). A new snow density parameterization for land data assimilation. *Journal of Hydrometeorology*, 18(1), 197–207. https://doi.org/10.1175/JHM-D-16-0166.1

Dawson, N., Broxton, P., & Zeng, X. (2018). Evaluation of remotely-sensed snow water equivalent and snow cover extent over the contiguous United States. *Journal of Hydrometeorology*. https://doi.org/10.1175/JHM-D-18-0007.1

Derksen, C., Toose, P., Rees, A., Wang, L., English, M., Walker, A., & Sturm, M. (2010). Development of a tundra-specific snow water equivalent retrieval algorithm for satellite passive microwave data. *Remote Sensing of Environment*, 114(8), 1699–1709. https://doi.org/10.1016/j.rse.2010.02.019

Dickinson, R. E. (1983). Land surface processes and climate−surface albedos and energy balance. In Theory of Climate, Advances in Geophysics, vol. 25; Saltzman, B., Ed.; Academic: San Diego, Calif, pp. 305−353.

Dong, J., Walker, J.P., Houser, P.R., & Sun, C. (2007). Scanning multichannel microwave radiometer snow water equivalent assimilation. Journal of Geophysical Research, 112(D7), D07108. https://doi.org/10.1029/2006JD007209

Dozier, J. (2011). Mountain hydrology, snow color, and the fourth paradigm. Eos, Trans. Amer. Geophys. Union, 92(43), 373−374, https://doi.org/10.1029/2011EO430001

Durand, M., & Margulis, S. A. (2006). Feasibility test of multifrequency radiometric data assimilation to estimate snow water equivalent. Journal of Hydrometeorology, 7(3), 443–457. https://doi.org/10.1175/JHM502.1

Durand, M., & Margulis, S. A. (2007). Correcting first-order errors in snow water equivalent estimates using a multifrequency, multiscale radiometric data assimilation scheme. *Journal of Geophysical Research*, 112(D13), D13121. https://doi.org/10.1029/2006JD008067

Durand, M., Kim, E. J, & Margulis, S. A. (2009). Radiance assimilation shows promise for snowpack characterization. *Geophysical Research Letters*, 36(2), L02503. https://doi.org/10.1029/2008GL035214

Dziubanski, D. J., & Franz, K. J. (2016). Assimilation of AMSR-E snow water equivalent data in a spatially-lumped snow model. *Journal of Hydrology*, 540, 26–39. https://doi.org/10.1016/j.jhydrol.2016.05.046

Ek, M.B., Mitchell, K.E., Lin, Y., Rogers, E., Grunmann, P., Koren, V., Gayno, G., & Tarpley, J.D. (2003). Implementation of Noah land surface model advances in the National Centers for Environmental Prediction operational mesoscale Eta model. *Journal of Geophysical Research*, 108(D22), 8851, https://doi.org/10.1029/2002JD003296

Evensen, G. (1994). Sequential data assimilation with a nonlinear quasi-geostrophic model using Monte Carlo methods to forecast error statistics. Journal of Geophysical Research, 99(C5), 10143–10162. https://doi.org/10.1029/94JC00572

Farr, Tom G., Paul A. Rosen, Edward Caro, Robert Crippen, Riley Duren, Scott Hensley, Michael Kobrick et al. (2007), The shuttle radar topography mission. *Reviews of Geophysics* 45(2).

Foster, J. L., Chang, A. T. C., Hall, D. K., & Rango, A. (1991). Derivation of snow water equivalent in boreal forests using microwave radiometry. *Arctic*, 44, 147–152. https://doi.org/10.14430/arctic1581

Foster, J. L., Sun, C., Walker, J. P., Kelly, R., Chang, A., Dong, J., & Powell, H. (2005). Quantifying the uncertainty in passive microwave snow water equivalent observations. *Remote Sensing of Environment*, 94(2), 187–203. https://doi.org/10.1016/j.rse.2004.09.012

Glynn, J. E., Carroll, T. R., Holman, P. B., & Grasty, R. L. (1988). An airborne gamma ray snow survey of a forested covered area with a deep snowpack, Remote Sensing of Environment, 26(2), 149-160.

Grenfell, T.C., Putkonen, J., (2008). A method for the detection of the severe rain-on-snow event on Banks Island, October 2003, using passive microwave remote sensing. *Water Resour. Res.* 44:3. http://dx.doi.org/10.1029/2007WR005929.

Hansen, M. & Song, X. P. (2018). Vegetation Continuous Fields (VCF) yearly global 0.05 deg. NASA EOSDIS Land Processes DAAC. https://doi.org/10.5067/MEaSUREs/VCF/VCF5KYR.001. [accessed on 1 March, 2019].

Imaoka, K., Kachi, M., Kasahara, M., Ito, N., Nakagawa, K., & Oki, T. (2010). Instrument performance and calibration of AMSR-E and AMSR2. International archives of the photogrammetry, remote sensing and spatial information science, 38(8), 13-18.

Jennings, K. S., Winchell, T. S., Livneh, B., & Molotch, N. P. (2018). Spatial variation of the rain-snow temperature threshold across the Northern Hemisphere. *Nature Communications*, 9, 1148, https://doi.org/10.1038/s41467-018-03629-7

Johnson, M. T., Ramage, J., Troy, T. J., & Brodzik, M. J. (2020). Snowmelt Detection with Calibrated, Enhanced- Resolution Brightness Temperatures (CETB) in Colorado Watersheds. Water Resources Research, 56(1).

Jordan, R. A. (1991). One-Dimensional Temperature Model for a Snow Cover. Technical Documentation for SNTHERM.89; Technical Report No. 91-16; U.S. Army Corps of Engineers: Washington, DC, USA.

Kelly, R. (2009). The AMSR-E snow depth algorithm: description and initial results. Journal of The Remote Sensing Society of Japan, 29(1), 307−317. https://doi.org/10.11440/rssj.29.307

Kelly, R., Chang, A., Tsang, L., & Foster, J. (2003). A prototype AMSR-E global snow area and snow depth algorithm. IEEE Transactions on Geoscience and Remote Sensing, 41(2), 230−242. https://doi.org/10.1109/TGRS.2003.809118

Kim, R. S., Kumar, S., Vuyovich, C., Houser, P., Lundquist, J., Mudryk, L.(2021). Snow Ensemble Uncertainty Project (SEUP): Quantification of snow water equivalent uncertainty across North America via ensemble land surface modeling. *The Cryosphere*, 15(2), 771-791.

Kumar, S. V., Peters-Lidard, C. D., Tian, Y., Houser, P. R., Geiger, J., Olden, S., Lighty, L., Eastman, J. L., Doty, B., Dirmeyer, P., Adams, J., Mitchell, K., Wood, E. F., & Sheffield, J. (2006). Land information system: An interoperable framework for high resolution land surface modeling. *Environmental Modelling & Software*, 21(10), 1402–1415, https://doi.org/10.1016/j.envsoft.2005.07.004

Kumar, S., Peters-Lidard, C., Tian, Y., Reichle, R. H., Geiger, J., Alonge, C., Eylander, J., & Houser, P. (2008). An integrated hydrologic modeling and data assimilation framework. *Computer*, 41(12), 52–59, https://doi.org/10.1109/MC.2008.511

Kumar, S. V., Peters-Lidard, C. D., Mocko, D., Reichle, R., Liu, Y., Arsenault, K.R., Xia, Y., Ek, M., Riggs, G., Livneh, B., & Cosh, M. (2014). Assimilation of remotely sensed soil moisture and snow depth retrievals for drought estimation. *Journal of Hydrometeorology*, 15(6), 2446–2469. https://doi.org/10.1175/JHM-D-13-0132.1

Kwon, Y., & Koo, B. K. (2014). Simulation of spatio-temporal distributions of winter soil temperature taking account of snow-melting and soil freezing-thawing processes. *Journal of Korea Water Resources Association*, 47(10), 945–958. http://dx.doi.org/10.3741/JKWRA.2014.47.10.945

Kwon, Y., Forman, B.A., Ahmad, J.A., Kumar, S.V., & Yoon, Y. (2019). Exploring the utility of machine learning-based passive microwave brightness temperature data assimilation over terrestrial snow in High Mountain Asia. *Remote Sensing*, 11(19), 2265. https://doi.org/10.3390/rs11192265

Kwon, Y., Toure, A.M., Yang, Z.–L., Rodell, M., & Picard, G. (2015). Error characterization of coupled land surface–radiative transfer models for snow microwave radiance assimilation. *IEEE Transactions on Geoscience and Remote Sensing*, 53(9), 5247–5268. https://doi.org/10.1109/TGRS.2015.2419977

Kwon, Y., Yang, Z.–L., Hoar, T.J., & Toure, A.M. (2017). Improving the radiance assimilation performance in estimating snow water storage across snow and land-cover types in North America. *Journal of Hydrometeorology*, 18(3), 651–668. https://doi.org/10.1175/JHM-D-16-0102.1

Kwon, Y., Yang, Z.–L., Zhao, L., Hoar, T. J., Toure, A.M., & Rodell, M. (2016). Estimating snow water storage in North America using CLM4, DART, and snow radiance data assimilation. *Journal of Hydrometeorology*, 17(11), 2853–2874. https://doi.org/10.1175/JHM-D-16-0028.1

Larue, F., Royer, A., De Séve, D., Roy, A., & Cosme, E. (2018a). Assimilation of passive microwave AMSR-2 satellite observations in a snowpack evolution model over northeastern Canada. *Hydrology and Earth System Sciences*, 22(11), 5711–5734. https://doi.org/10.5194/hess-22-5711-2018

Larue, F., Royer, A., De Séve, D., Roy, A., Picard, G., Vionnet, V., & Cosme, E. (2018b). Simulation and assimilation of passive microwave data using a snowpack model coupled to a calibrated radiative transfer model over northeastern Canada. *Water Resources Research*, 54(7), 4823–4848. https://doi.org/10.1029/2017WR022132

Lemmetyinen, J., Derksen, C., Toose, P., Proksch, M., Pulliainen, J., Kontu, A., Rautiainen, K., Seppänen, J., & Hallikainen, M. (2015). Simulating seasonally and spatially varying snow cover brightness temperature using HUT snow emission model and retrieval of a microwave effective grain size. *Remote Sensing of Environment*, 156, 71–95. https://doi.org/10.1016/j.rse.2014.09.016

Letcher, T., Naple, P., Minder, J.R., Rafieeinasab, A., Enzminger, T., Dugger, A.L., and Gochis, D. (2021). Using a high-density network of surface meteorological stations to evaluate and improve the simulation of snow in Noah-MP over the Northeastern United States to improve regional National Water Model performance. *35th Conference on Hydrology, 101st American Meteorological Society Annual Meeting*.

Liu, Y., Peters-Lidard, C., Kumar, S., Foster, J., Shaw, M., Tian, Y., & Fall, G. (2013). Assimilating satellite-based snow depth and snow cover products for improving snow predictions in Alaska. *Advances in Water Resources*, 54, 208–227. https://doi.org/doi:10.1016/j.advwatres.2013.02.005

Musselman, K. N., Addor, N., Vano, J. A., & Molotch, N. P. (2021). Winter melt trends portend widespread declines in snow water resources. *Nature Climate Change*, 11(5), 418-424.

Niu, G. –Y. & Yang, Z. –L. (2004). The effects of canopy processes on snow surface energy and mass balances. *Journal of Geophysical Research*, 109(D23), D23111, https://doi.org/10.1029/2004JD004884

Niu, G. –Y. & Yang, Z. –L. (2006). Effects of frozen soil on snowmelt runoff and soil water storage at a continental scale. *Journal of Hydrometeorology*, 7(5), 937–952, https://doi.org/10.1175/JHM538.1

Niu, G. –Y., Yang, Z. –L., Dickinson, R. E., Gulden, L. E., & Su, H. (2007). Development of a simple groundwater model for use in climate models and evaluation with Gravity Recovery and Climate Experiment data. *Journal of Geophysical Research*, 112(D7), D07103, https://doi.org/10.1029/2006JD007522

Niu, G. –Y., Yang, Z. –L., Mitchell, K. E., Chen, F., Ek, M. B., Barlage, M., Kumar, A., Manning, K., Niyogi, D., Rosero, E., Tewari, M., & Xia, Y. (2011). The community Noah land surface model with multiparameterization options (Noah- MP): 1. Model description and evaluation with local- scale measurements. *Journal of Geophysical Research*, 116(D12), D12109, https://doi.org/10.1029/2010JD015139

Peck, E. L., Bissell, V. C., Jones, E. B., & Burge, D. L. (1971). Evaluation of snow water equivalent by airborne measurement of passive terrestrial gamma radiation. *Water Resources Research*, 7(5), 1151–1159.

Peck, E. L., Carroll, T. R., & VanDemark, S. C. (1980). Operational aerial snow surveying in the United States/Etude de neige aérienne effectuée aux Etats Unis. *Hydrological Sciences Journal*, 25(1), 51–62

Peters-Lidard, C. D., Houser, P. R., Tian, Y., Kumar, S. V., Geiger, J., Olden, S., Lighty, L., Doty, B., Dirmeyer, P., Adams, J., Mitchell, K., Wood, E. F., & Sheffield, J. High-performance Earth system modeling with NASA/GSFC's Land Information System. *Innovations in Systems and Software Engineering*, 3, 157–165, https://doi.org/10.1007/s11334-007-0028-x

Reichle, R. H., Walker, J. P., Koster, R. D., & Houser, P. R. (2002). Extended versus ensemble Kalman filtering for land data assimilation. *Journal of Hydrometeorology*, 3(6), 728–740, https://doi.org/10.1175/1525-7541(2002)003<0728:EVEKFF>2.0.CO;2

Roy, A., Royer, A., Wigneron, J.–P., Langlois, A., Bergeron, J., & Cliche, P. (2012). A simple parameterization for a boreal forest radiative transfer model at microwave frequencies. Remote Sensing of Environment, 124, 371–383. https://doi.org/10.1016/j.rse.2012.05.020

Semmens, K.A., Ramage, J., Bartsch, A., Liston, G.E., 2013. Early snowmelt events: detection, distribution, and significance in a major sub-arctic watershed. Environ. Res. Lett. 8, 11.

Sellers, P. J. (1985). Canopy reflectance, photosynthesis and transpiration. *International Journal of Remote Sensing*, 6(8), 1335–1372, https://doi.org/10.1080/01431168508948283

Smyth, E. J., Raleigh, M. S., & Small, E. E. (2020). Improving SWE Estimation with Data Assimilation: The Influence of Snow Depth Observation Timing and Uncertainty. Water Resources Research, 56(5), e2019WR026853.

Sturm, M., Taras, B., Liston, G. E., Derksen, C., Jonas, T., & Lea, J. (2010). Estimating snow water equivalent using snow depth data and climate classes. *Journal of Hydrometeorology*, 11(6), 1380-1394. https://doi.org/10.1175/2010JHM1202.1

Sturm, M., & Liston, G. E. (2021). Revisiting the Global Seasonal Snow Classification: An Updated Dataset for Earth System Applications. Journal of Hydrometeorology, 22(11), 2917-2938.

Sturm, M., Goldstein, M. A., & Parr, C. (2017). Water and life from snow: A trillion dollar science question. *Water Resources Research*, 53(5), 3534-3544.

Suzuki, K. & Zupanski, M. (2018). Uncertainty in solid precipitation and snow depth prediction for Siberia using the Noah and Noah-MP land surface models. *Frontiers of Earth Science*, 12, 672–682. https://doi.org/10.1007/s11707-018-0691-2

Tuttle, S. E., Jacobs, J. M., Vuyovich, C. M., Olheiser, C., & Cho, E. (2018). Intercomparison of snow water equivalent observations in the Northern Great Plains. *Hydrological Processes*, 32(6), 817-829. https://doi.org/10.1002/hyp.11459

Tuttle, S. E., & Jacobs, J. M. (2019). Enhanced identification of snow melt and refreeze events from passive microwave brightness temperature using air temperature. Water Resources Research, 55(4), 3248-3265.

Vogel, R. M., Carroll, T. R., & Carroll, S. S. (1985), Simulation of airborne snow water equivalent measurement errors made over a forest environment, *Proceedings of the American Society of Civil Engineers Symposium*, Denver, CO, p. 9.

Vuyovich, C. M., Jacobs, J. M., Hiemstra, C. A., & Deeb, E. J. (2017). Effect of spatial variability of wet snow on modeled and observed microwave emissions. *Remote Sensing of Environment*, 198, 310-320. https://doi.org/10.1016/j.rse.2017.06.016

Walker, A.E. & Goodison, B.E. (1993). Discrimination of a wet snow cover using passive microwave satellite data. *Anuals of Glaciology*, 17, 307–311. https://doi.org/10.3189/S026030550001301X

Welty, J., & Zeng, X. (2021). Characteristics and causes of extreme snowmelt over the conterminous United States. Bulletin of the American Meteorological Society, 102(8), E1526-E1542.

Wilson, M.F.J., O'Connell, B., Brown, C., Guinan, J.C., Grehan, A.J. (2007). Multiscale terrain analysis of multibeam bathymetry data for habitat mapping on the continental slope. Marine Geodesy 30: 3-35.

Wrzesien, M. L., Kumar, S.V., Vuyovich, C.M., Gutmann, E.D., Kim, R.-S., Forman, B.A., Durand, M. Raleigh, M.S., Webb, R., & Houser, P. (2021). Development of a "nature run" for observing system simulation experiments (OSSEs) for snow mission development, *Journal of Hydrometeorology, under review.*

Xia, Y., Mocko, D., Huang, M., Li, B., Rodell, M., Mitchell, K. E., Cai, X., & Ek, M. B. (2017). Comparison and assessment of three advanced land surface models in simulating terrestrial water storage components over the United States. *Journal of Hydrometeorology*, 18(3), 625–649. https://doi.org/10.1175/JHM-D-16-0112.1

Xue, Y., Forman, B. A., & Reichle, R.H. (2018). Estimating snow mass in North America through assimilation of Advanced Microwave Scanning Radiometer brightness temperature observations using the Catchment land surface model and support vector machines. *Water Resources Research*, 54 (9), 6488–6509. https://doi.org/10.1029/2017WR022219

Yang, R. & Friedl, M.A. (2003). Modeling the effects of three-dimensional vegetation structure on surface radiation and energy balance in boreal forests. *Journal of Geophysical Research*, 108(D16), 8615. https://doi.org/10.1029/2002JD003109

Yang, Z. –L. & Dickinson, R. E. (1996). Description of the Biosphere-Atmosphere Transfer Scheme (BATS) for the soil moisture workshop and evaluation of its performance. *Global Planetary Change*i, 13(1-4), 117–134, https://doi.org/10.1016/0921-8181(95)00041-0

Yang, Z. –L., Niu, G. –Y., Mitchell, K. E., Chen, F., Ek, M. B., Barlage, M., Longuevergne, L., Manning, K., Niyogi, D., Tewari, M., & Xia, Y. (2011). The community Noah land surface model with multiparameterization options (Noah-MP): 2. Evaluation over global river basins. *Journal of Geophysical Research*, 116(D12), D12110, https://doi.org/10.1029/2010JD015140

Zeng, X., Broxton, P., & Dawson, N. (2018). Snowpack change from 1982 to 2016 over conterminous United States. *Geophysical Research Letters*, 45, 12,940–12,947. https://doi.org/10.1029/2018GL079621

Zhang, X. Y., Jin, J., Zeng, X., Hawkins, C. P., Neto, A. A., & Niu, G. Y. (2022). The Compensatory CO2 Fertilization and Stomatal Closure Effects on Runoff Projection From 2016–2099 in the Western United States. Water Resources Research, 58(1), e2021WR030046.